

Chapter 5

Weak Decays of Open Flavor Mesons

5.1 Introduction

Charm sector is a good platform to test the absolute scale of computed decay amplitudes in terms of form factors because the Cabibbo-Kobayashi-Maskawa (CKM) matrix elements can be determined independently for D decays by exploiting the CKM unitarity and numerical values of the matrix elements for B decays. Study of charm decays is also important for understanding of new physics (NP) affecting the up-type quark dynamics as it is the only up-type quark displaying flavor oscillations [263, 264]. Some hints about the dynamics of TeV scale QCD are expected from charm flavour oscillations in the same line of charm mass and dynamics predictions from experimentally observed low energy kaon oscillations [265]. These flavour oscillations are very sensitive probes for the underlying new physics interactions involving charged particles.

Semileptonic decays have reasonably large amplitudes making them more accessible in recently upgraded experimental facilities and hence are considered to be primary source to get information about CKM matrix elements. Charmed meson semileptonic decays are the easiest direct way to determine the magnitude of quark-mixing parameters i.e. direct access to $|V_{cs}|$ and $|V_{cd}|$. The study of charm semileptonic decays provides insight to $|V_{cq}|^2$ via matrix elements that describe strong interaction effects and may contribute to a precise determination of the CKM matrix element $|V_{ub}|$ via constraints provided by charm decays to reduce the model dependence in extracting $|V_{ub}|$ from exclusive charmless B semileptonic decays. For example, flavour symmetry relates the form factors of the semileptonic decays of D and B

systems. Recently, the matrix elements $|V_{cd(s)}|$ was extracted (PDG [1]) from the experimental results from the *BABAR* [266,267], Belle [268], BESIII [269], CLEO [270] in the channel $D \rightarrow \pi(K)\ell^+\nu_\ell$.

Many lattice quantum chromodynamics (LQCD) papers are available in literature regarding the semileptonic form factors for the channel $D \rightarrow (K, \pi)\ell\nu_\ell$. However, in the light sector of daughter meson, the first successful computation of form factors for $D_s \rightarrow \phi\ell^+\nu_\ell$ from full LQCD was reported by HPQCD collaboration [21]. Later, $D_s \rightarrow \eta^{(\prime)}\ell^+\nu_\ell$ semileptonic form factors were also reported for the first time using LQCD [22]. The heavy ($D_{(s)}$) to light ($\pi, \rho, \omega, \phi, \eta^{(\prime)}, K$) form factors have also been computed within the QCD sum rules [271,272] and light cone QCD sum rules (LCSR) [273–276]. The LCSR along with heavy quark effective theory (HQET) has also been employed for computing the transition form factors and branching fractions [277]. Recently, computation of form factors and semileptonic branching fractions of $D \rightarrow \rho$ decays have been reported using LCSR with chiral correlator [278]. The heavy to light form factors are also computed in the heavy quark limit of the large energy effective theory [279], constituent quark model [280], chiral quark model (χ QM) [281] and chiral perturbation theory [282]. The form factors and semileptonic branching fractions of $D_{(s)}$ mesons are also computed in the framework of heavy meson chiral theory (HM χ T) [283,284] and the light front quark model (LFQM) [285–287]. The authors of Ref. [288] have computed the semileptonic branching fractions of $D_{(s)}$ mesons in the chiral unitary (χ UA) approach.

In this chapter, we compute the semileptonic branching fractions of the charmed (D) and charmed-strange (D_s^+) meson to light mesons ($\rho, \omega, \phi, \eta^{(\prime)}$ and $K^{(*0)}$). The required transition form factors are computed in the framework of Covariant Confinement Quark Model (CCQM) [57,58,289]. The CCQM is the effective field theory approach with the infrared confinement for the hadronic interactions with their constituents. This allows us to compute the form factors in the complete physical range of momentum transfer. We also compute the semileptonic branching fractions for $D_{(s)}^+ \rightarrow D^0 e^+ \nu_e$. These are the rare class of semileptonic decays where the light quark decays weakly leaving behind the heavy quark as a spectator. Recently, BESIII collaboration has reported the upper bound on the branching fraction for the channel $D^+ \rightarrow D^0 e^+ \nu_e$ at 90% confidence level to be 1.0×10^{-4} [290]. These channels were studied within the SU(3) symmetry [291] as well as heavy flavour conserving decays [292].

The next section gives detailed formulation of the model CCQM. Next, we provide the branching fractions in terms of helicity structure functions followed by the results in comparison with the experimental data and theoretical predictions. This study comprising computation of leptonic and semileptonic decays of D and $D_{(s)}$ mesons is published in Physical Review D [293,294]. In these papers, we have considered the channels $D^0 \rightarrow (K^-, \pi^-, \rho^-, K^*(892)^-)\ell^+\nu_\ell$, $D^+ \rightarrow (\bar{K}^0, \pi^0, \eta, \eta', \rho^0, \omega, \bar{K}^*(892)^0)\ell^+\nu_\ell$ and $D_s^+ \rightarrow (K^0, \eta, \eta', \phi, K^*(892)^-)\ell^+\nu_\ell$ for $\ell = e$ and μ .

5.2 Methodology

The CCQM is an effective quantum field approach [57, 58, 289] for hadronic interactions that utilizes an effective Lagrangian for hadrons interacting with the constituent quarks. In this model it is assumed that hadrons interact with the constituent quarks only. The Lagrangian describing the coupling of meson $M(q_1\bar{q}_2)$ to its constituent quarks q_1 and \bar{q}_2 is given by

$$\mathcal{L}_{int} = g_M M(x) \int dx_1 \int dx_2 F_M(x; x_1, x_2) \bar{q}_2(x_2) \Gamma_M q_1(x_1) + H.c. \quad (5.1)$$

where Γ_M is the Dirac matrix and projects onto the spin quantum number of relevant mesonic field $M(x)$. F_M is the vertex factor which characterizes the finite size of the meson and is invariant under translation $F_M(x+a, x_1+a, x_2+a) = F_M(x, x_1, x_2)$. This ensures the Lorentz invariance of the Lagrangian Eq. (5.1) for any value of four-vector a . We choose the following form of the vertex function

$$F_M(x, x_1, x_2) = \delta^{(4)}\left(x - \sum_{i=1}^2 w_i x_i\right) \Phi_M((x_1 - x_2)^2) \quad (5.2)$$

with Φ_M is the correlation function of two constituent quarks with masses m_{q_1} and m_{q_2} and $w_{q_i} = m_{q_i}/(m_{q_1} + m_{q_2})$ such that $w_1 + w_2 = 1$.

We choose Gaussian function for vertex function as

$$\tilde{\Phi}_M(-p^2) = \exp(p^2/\Lambda_M^2) \quad (5.3)$$

with the parameter Λ_M characterized by the finite size of the meson. Note that any form of Φ_M is appropriate as long as it falls off sufficiently fast in the ultraviolet region of Euclidian space in order to overcome the ultraviolet divergence of the loop integral. The local fermion propagator for the constituent quarks is given by

$$S_q(k) = \frac{1}{m_q - \not{k}} \quad (5.4)$$

with an effective constituent quark mass m_q . The compositeness condition [59, 60]

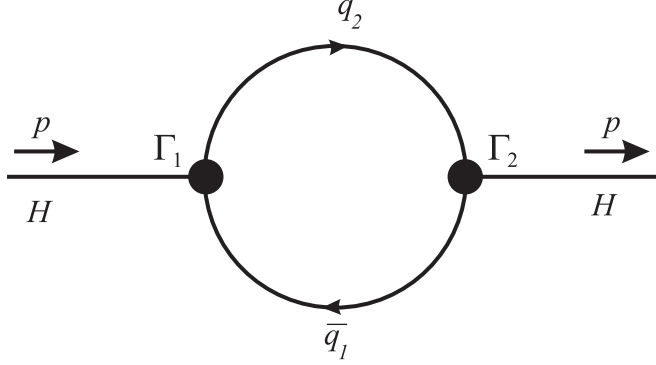


Figure 5.1: Diagram describing meson mass operator.

is used to determine the coupling constant g_M in Eq. (5.1)

$$Z_M = 1 - \frac{3g_M^2}{4\pi^2} \tilde{\Pi}'_M(m_M^2) = 0, \quad (5.5)$$

where $\tilde{\Pi}'_M(p^2)$ is the derivative of the mass operator taken on the mass-shell $p^2 = m_M^2$. By using the Fourier transformation of the vertex function in Eq. (5.3) and quark propagator in Eq. (5.4), one can write the meson mass function defined in Fig. 5.1. For pseudoscalar meson

$$\tilde{\Pi}_P(p^2) = N_c g_P^2 \int \frac{d^4 k}{(2\pi)^4 i} \tilde{\Phi}_P^2(-k^2) \text{tr} \left(\gamma^5 S_1(k + w_1 p) \gamma^5 S_2(k - w_2 p) \right), \quad (5.6)$$

and for vector meson

$$\tilde{\Pi}_V^{\mu\nu}(p^2) = N_c g_V^2 \int \frac{d^4 k}{(2\pi)^4 i} \tilde{\Phi}_V^2(-k^2) \text{tr} \left(\gamma^\mu S_1(k + w_1 p) \gamma^\nu S_2(k - w_2 p) \right) \quad (5.7)$$

where $N_c = 3$ is the number of colors. Since the vector meson is on its mass-shell, one has $\epsilon_V \cdot p = 0$ and needs only the part of the vector meson function proportional to $g_{\mu\nu}$, given by

$$\tilde{\Pi}_V(p^2) = \frac{1}{3} \left(g_{\mu\nu} - \frac{p_\mu p_\nu}{p^2} \right) \tilde{\Pi}_V^{\mu\nu}(p). \quad (5.8)$$

The loop integrations in Eqs. (5.6) and (5.7) are performed with Fock-Schwinger representation of quark propagators

$$\begin{aligned} S_q(k+p) &= \frac{1}{m_q - \not{k} - \not{p}} = \frac{m_q + \not{k} + \not{p}}{m_q^2 - (k+p)^2} \\ &= (m_q + \not{k} + \not{p}) \int_0^\infty d\alpha e^{-\alpha[m_q^2 - (k+p)^2]}, \end{aligned} \quad (5.9)$$

allowing tensor loop integral by conversion of the loop momentum to the derivative of the exponential function. All the loop integrations are performed in Euclidean space transformed from Minkowski space using the Wick rotation

$$k_0 = e^{i\frac{\pi}{2}} k_4 = ik_4 \quad (5.10)$$

so that $k^2 = k_0^2 - \vec{k}^2 = -k_4^2 - \vec{k}^2 = -k_E^2 \leq 0$. Simultaneously one has to rotate all external momenta, i.e. $p_0 \rightarrow ip_4$ so that $p^2 = -p_E^2 \leq 0$. Then the quadratic form in Eq. (5.9) becomes positive-definite,

$$m_q^2 - (k + p)^2 = m_q^2 + (k_E + p_E)^2 > 0 \quad (5.11)$$

where the integral over α is convergent.

Collecting the representation of the vertex function Eq. (5.3) and quark propagator Eq. (5.4), we perform the Gaussian integration in the derivatives of the mass functions in Eqs. (5.6) and (5.7). The exponential function has the form $ak^2 + 2kr + z_0$, where $r = bp$. Using the following properties

$$\begin{aligned} k^\mu \exp(ak^2 + 2kr + z_0) &= \frac{1}{2} \frac{\partial}{\partial r_\mu} \exp(ak^2 + 2kr + z_0), \\ k^\mu k^\nu \exp(ak^2 + 2kr + z_0) &= \frac{1}{2} \frac{\partial}{\partial r_\mu} \frac{1}{2} \frac{\partial}{\partial r_\nu} \exp(ak^2 + 2kr + z_0), \text{ etc.} \end{aligned}$$

one can replace k by $\not{\partial}_r = \gamma^\mu \frac{\partial}{\partial r_\mu}$ in order to perform the exchange of tensor integrations for differentiation of the Gaussian exponent. The r -dependent Gaussian exponent $e^{-r^2/a}$ can be moved to the left through the differential operator $\not{\partial}_r$ using

$$\begin{aligned} \frac{\partial}{\partial r_\mu} e^{-r^2/a} &= e^{-r^2/a} \left[-\frac{2r^\mu}{a} + \frac{\partial}{\partial r_\mu} \right], \\ \frac{\partial}{\partial r_\mu} \frac{\partial}{\partial r_\nu} e^{-r^2/a} &= e^{-r^2/a} \left[-\frac{2r^\mu}{a} + \frac{\partial}{\partial r_\mu} \right] \cdot \left[-\frac{2r^\nu}{a} + \frac{\partial}{\partial r_\nu} \right], \text{ etc.} \end{aligned} \quad (5.12)$$

Finally, we move the derivatives to the right by using the commutation relation

$$\left[\frac{\partial}{\partial r_\mu}, r^\nu \right] = g^{\mu\nu}. \quad (5.13)$$

The last step has been done by using a FORM code [295] which works for any numbers of loops and propagators. In the remaining integrals over the Fock-Schwinger parameters $0 \leq \alpha_i < \infty$, we introduce an additional integration which converts the set of Fock-Schwinger parameters into a simplex. Using the transformation [296]

$$\prod_{i=1}^n \int_0^\infty d\alpha_i f(\alpha_1, \dots, \alpha_n) = \int_0^\infty dt t^{n-1} \prod_{i=1}^n \int d\alpha_i \delta \left(1 - \sum_{i=1}^n \alpha_i \right) f(t\alpha_1, \dots, t\alpha_n) \quad (5.14)$$

Finally, we have

$$\begin{aligned}
\tilde{\Pi}_M(p^2) &= \frac{3g_M^2}{4\pi^2} \int_0^\infty \frac{dt}{a_M^2} \int_0^1 d\alpha e^{-tz_0+z_M} f_M(t, \alpha), & (5.15) \\
z_0 &= \alpha m_{q_1}^2 + (1-\alpha)m_{q_2}^2 - \alpha(1-\alpha)p^2, \\
z_M &= \frac{2s_M t}{2s_M + t} (\alpha - w_2)^2 p^2, \\
a_M &= 2s_M + t, \quad b = (\alpha - w_2)t.
\end{aligned}$$

where $S_M = 1/\Lambda_M^2$ and the function $f_M(t, \alpha)$ coming from the trace evaluation in Eqs. (5.6) and (5.7).

It can be seen that the integral over t in Eq. (5.15) is well defined and convergent below the threshold $p^2 < (m_{q_1} + m_{q_2})^2$. The convergence of the integral above threshold $p^2 \geq (m_{q_1} + m_{q_2})^2$ is ensured by incrementing the quark mass by an imaginary part, i.e. $m_q \rightarrow m_q - i\epsilon$, $\epsilon > 0$, in the quark propagator Eq. (5.4). This allows transformation of the integration variable t to imaginary axis $t \rightarrow it$. As a result, the integral Eq. (5.15) becomes convergent, however it does obtain an imaginary part that accounts for quark pair production.

However, by truncating the scale of integration to the upper limit by introducing the infrared cutoff

$$\int_0^\infty dt(\dots) \rightarrow \int_0^{1/\lambda^2} dt(\dots), \quad (5.16)$$

all possible thresholds present in the initial quark diagram can be removed [289]. Thus the infrared cutoff parameter λ ensures the confinement. This method is quite general and can be used for diagrams with an arbitrary number of loops and propagators. In CCQM, the infrared cutoff parameter λ is taken to be universal for all physical processes.

Since the model CCQM is not based on the first principle, we need to fix the parameters such as quark masses (m_q) and meson size parameters (Λ_M) as in Tab. 5.1 and Tab. 5.2 respectively. The model parameters are determined by fitting computed leptonic and radiative decay constants to available experimental data or LQCD for pseudoscalar and vector mesons. The matrix elements of the leptonic decays are described by the Feynman diagram shown in Fig. 5.2. The leptonic decay constants

Table 5.1: Quark masses and infrared cutoff parameter in GeV

$m_{u/d}$	m_s	m_c	m_b	λ
0.241	0.428	1.672	5.05	0.181

Table 5.2: Meson size parameters in GeV

Λ_D	Λ_{D_s}	Λ_K	Λ_{K^*}	Λ_ϕ	Λ_ρ	Λ_ω	Λ_π	$\Lambda_\eta^{q\bar{q}}$	$\Lambda_\eta^{s\bar{s}}$	$\Lambda_{\eta'}^{q\bar{q}}$	$\Lambda_{\eta'}^{s\bar{s}}$
1.600	1.784	1.014	0.805	0.883	0.624	0.488	0.870	0.881	1.973	0.257	2.797

of the pseudoscalar and vector mesons are defined by

$$\begin{aligned}
 N_c g_P \int \frac{d^4 k}{(2\pi)^4 i} \tilde{\phi}_P(-k^2) \text{tr}[O^\mu S_1(k + w_1 p) \gamma^5 S_2(k - w_2 p)] &= f_p p^\mu \\
 N_c g_V \int \frac{d^4 k}{(2\pi)^4 i} \tilde{\phi}_V(-k^2) \text{tr}[O^\mu S_1(k + w_1 p) \not{k} S_2(k - w_2 p)] &= m_V f_V \epsilon_V^\mu \quad (5.17)
 \end{aligned}$$

where N_c is the number of colors and $O^\mu = \gamma^\mu(1 - \gamma_5)$ is the weak Dirac matrix with left chirality. Our results for the leptonic decay constants are given in the Table 5.3.

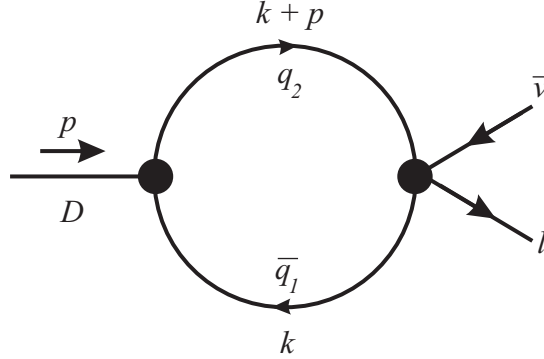


Figure 5.2: Quark model diagrams for the D -meson leptonic decay

The decay constants we use in our calculations match quite well with PDG, LQCD and QCD sum rules (QCDSR) parameters.

In the SM, pure leptonic decays $D_{(s)}^+ \rightarrow \ell \nu_\ell$ proceed by exchange of virtual W boson. The leptonic branching fraction is given by

$$B(D_{(s)}^+ \rightarrow \ell \nu_\ell) = \frac{G_F^2}{8\pi} m_{D_{(s)}} m_\ell^2 \left(1 - \frac{m_\ell^2}{m_{D_{(s)}}^2}\right)^2 f_{D_{(s)}}^2 |V_{cd}|^2 \tau_{D_{(s)}} \quad (5.18)$$

where, G_F is the fermi coupling constant, m_D and m_ℓ are the D -meson and lepton masses respectively and $\tau_{D_{(s)}}$ is the $D_{(s)}$ -meson lifetime. $f_{D_{(s)}}$ is the leptonic decay constant of D -meson from Table 5.3. The resultant branching fractions for $\ell = \tau, \mu$

Table 5.3: Leptonic decay constants f_H (in MeV)

f_H	Present	Data	Reference
f_D	206.08	202.2 (2.2) (2.6)	LQCD [297]
		210 ± 11	QCDSR [298]
		211.9(1.1)	PDG [1]
f_{D_s}	257.70	258.7 (1.1) (2.9)	LQCD [297]
		259 ± 10	QCDSR [298]
		249.0(1.2)	PDG [1]
f_{D_s}/f_D	1.25	1.173(3)	PDG [1]
f_K	156.96	155.37(34)	LQCD [299]
		157.9 ± 1.5	LQCD [300]
		155.6(0.4)	PDG [1]
f_π	130.30	130.39 (20)	LQCD [299]
		132.3 ± 1.6	LQCD [300]
		130.2(1.7)	PDG [1]
f_K/f_π	1.20	1.1928(26)	PDG [1]
f_{D^*}	244.27	$278 \pm 13 \pm 10$	LQCD [301]
		263 ± 21	QCDSR [298]
$f_{D_s^*}$	272.08	311 ± 9	LQCD [301]
		308 ± 21	QCDSR [298]
f_{K^*}	226.81	222 ± 8	QCDSR [302]
f_ρ	218.28	$208.5 \pm 55 \pm 0.9$	LQCD [303]
f_ϕ	226.56	238 ± 3	LQCD [304]
		215 ± 5	QCDSR [302]
f_ω	198.38	194.60 ± 3.24	LFQM [286]

and e are given in Table 5.4. It is important to note here that the branching fractions are affected by different lepton masses through the helicity flip factor $(1 - m_\ell^2/m_{D(s)}^2)^2$.

 Table 5.4: Leptonic $D_{(s)}^+$ branching fractions

Channel	Present	PDG Data [1]
$D^+ \rightarrow e^+ \nu_e$	8.42×10^{-9}	$< 8.8 \times 10^{-6}$
$D^+ \rightarrow \mu^+ \nu_\mu$	3.57×10^{-4}	$(3.74 \pm 0.17) \times 10^{-4}$
$D^+ \rightarrow \tau^+ \nu_\tau$	0.95×10^{-3}	$< 1.2 \times 10^{-3}$
$D_s^+ \rightarrow e^+ \nu_e$	1.40×10^{-7}	$< 8.3 \times 10^{-5}$
$D_s^+ \rightarrow \mu^+ \nu_\mu$	5.97×10^{-3}	$(5.50 \pm 0.23) \times 10^{-3}$
$D_s^+ \rightarrow \tau^+ \nu_\tau$	5.82 %	$(5.48 \pm 0.23)\%$

5.3 Form factors and differential decay distribution

After fixing all the model parameters, we employ CCQM to compute the semileptonic branching fractions of $D_{(s)} \rightarrow P/V$ transition where P and V corresponds to pseudoscalar and vector daughter mesons. We start with the definitions of the form factors. The invariant matrix element for this decay can be written as

$$M(D_{(s)} \rightarrow (P, V)\ell^+\nu_\ell) = \frac{G_F}{\sqrt{2}}V_{cx}\langle(P, V)|\bar{x}\gamma^\mu(1 - \gamma_5)c|D_{(s)}\rangle\ell^+O^\mu\nu_\ell \quad (5.19)$$

where $O^\mu = \gamma_\mu(1 - \gamma_5)$ and $x = d, s$. The matrix elements for the above semileptonic transitions in the covariant quark model are defined by the diagram in Fig 5.3. The

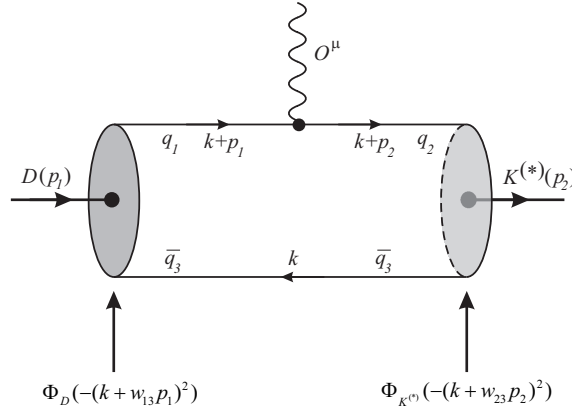


Figure 5.3: Quark model diagrams for the D -meson semileptonic decay

matrix element for the semileptonic transition can be written as

$$\begin{aligned} \langle P(p_2)|\bar{x}O^\mu c|D_{(s)}(p_1)\rangle &= N_c g_{D_{(s)}} g_P \int \frac{d^4k}{(2\pi)^4 i} \tilde{\Phi}_{D_{(s)}}(-(k+w_{13}p_1)^2) \tilde{\Phi}_P(-(k+w_{23}p_2)^2) \\ &\quad \times \text{tr}[O^\mu S_1(k+p_1)\gamma^5 S_3(k)\gamma^5 S_2(k+p_2)] \\ &= F_+(q^2)P^\mu + F_-(q^2)q^\mu \end{aligned} \quad (5.20)$$

$$\begin{aligned} \langle V(p_2, \epsilon_\nu)|\bar{x}O^\mu c|D_{(s)}(p_1)\rangle &= N_c g_{D_{(s)}} g_V \int \frac{d^4k}{(2\pi)^4 i} \tilde{\Phi}_{D_{(s)}}(-(k+w_{13}p_1)^2) \tilde{\Phi}_V(-(k+w_{23}p_2)^2) \\ &\quad \times \text{tr}[O^\mu S_1(k+p_1)\gamma^5 S_3(k)\not{\epsilon}_\nu^\dagger S_2(k+p_2)] \\ &= \frac{\epsilon_\nu^\dagger}{m_1+m_2} [-g^{\mu\nu}P \cdot q A_0(q^2) + P^\mu P^\nu A_+(q^2) \\ &\quad + q^\mu P^\nu A_-(q^2) + i\varepsilon^{\mu\nu\alpha\beta} P_\alpha q_\beta V(q^2)] \end{aligned} \quad (5.21)$$

with $P = p_1 + p_2$, $q = p_1 - p_2$ and ϵ_ν to be the polarization vector such that $\epsilon_\nu^\dagger \cdot p_2 = 0$ and on-shell conditions of particles require $p_1^2 = m_1^2 = m_{D_{(s)}}^2$ and $p_2^2 = m_2^2 = m_{P,V}^2$. Since there are three quarks involved in this transition, we use $w_{ij} = m_{q_j}/(m_{q_i} + m_{q_j})$

($i, j = 1, 2, 3$) such that $w_{ij} + w_{ji} = 1$. Performing the loop integration in Eqs (5.20) and (5.21), we obtain the semileptonic form factors within the entire range of momentum transfer $0 \leq q^2 \leq q_{max}^2$ with $q_{max}^2 = (m_{D(s)} - m_{P,V})^2$. The required multi-dimensional integration appeared in Eqs. (5.20) and (5.21) are computed numerically using *Mathematica* as well as FORTRAN codes with NAG library. We also represent our form factors using double pole parametrization as

$$F(q^2) = \frac{F(0)}{1 - as + bs^2}, \quad s = \frac{q^2}{m_1^2} \quad (5.22)$$

In Tab. 5.5, we list the quark channel and the CKM matrix for the semileptonic decays of $D_{(s)}$ mesons and in Tab. 5.6, we give the numerical results of the form factors and associated double pole parameters. For the comparison of our form

Table 5.5: Quark channel and associated CKM matrix element for semileptonic decays ($\phi = 39.3$ deg)

Channel	qq_1	qq_2	V_{ckm}	Channel	qq_1	qq_2	V_{ckm}
$D^0 \rightarrow K^-$	$c\bar{u}$	$s\bar{u}$	V_{cs}	$D^+ \rightarrow K^0$	$c\bar{d}$	$s\bar{d}$	V_{cs}
$D^0 \rightarrow K^*(892)^-$	$c\bar{u}$	$s\bar{u}$	V_{cs}	$D^+ \rightarrow K^*(892)^0$	$c\bar{d}$	$s\bar{d}$	V_{cs}
$D_s^+ \rightarrow K^0$	$c\bar{s}$	$d\bar{s}$	V_{cd}	$D_s^+ \rightarrow K^*(892)^0$	$c\bar{s}$	$d\bar{s}$	V_{cd}
$D^0 \rightarrow \pi^-$	$c\bar{u}$	$d\bar{u}$	V_{cd}	$D^+ \rightarrow \pi^0$	$c\bar{d}$	$d\bar{d}$	$V_{cd}/\sqrt{2}$
$D^0 \rightarrow \rho^-$	$c\bar{u}$	$d\bar{u}$	V_{cd}	$D^+ \rightarrow \rho^0$	$c\bar{d}$	$d\bar{d}$	$-V_{cd}/\sqrt{2}$
$D^+ \rightarrow \omega$	$c\bar{d}$	$d\bar{d}$	$V_{cd}/\sqrt{2}$	$D_s^+ \rightarrow \phi$	$c\bar{s}$	$s\bar{s}$	V_{cs}
$D^+ \rightarrow \eta$	$c\bar{d}$	$d\bar{d}$	$V_{cd} \cos \phi / \sqrt{2}$	$D_s^+ \rightarrow \eta$	$c\bar{s}$	$s\bar{s}$	$V_{cs} \sin \phi$
$D^+ \rightarrow \eta'$	$c\bar{d}$	$d\bar{d}$	$V_{cd} \sin \phi / \sqrt{2}$	$D_s^+ \rightarrow \eta'$	$c\bar{s}$	$s\bar{s}$	$V_{cs} \cos \phi$
$D^+ \rightarrow D^0$	$c\bar{d}$	$c\bar{u}$	V_{ud}	$D_s^+ \rightarrow D^0$	$c\bar{s}$	$c\bar{u}$	V_{us}

factors with the other studies, we need to transform our form factors to the Bauer-Stech-Wirbel (BSW) form factors. The relation reads [305]

$$\begin{aligned} A'_2 &= A_+, \quad V' = V \\ A'_1 &= \frac{M_1 - M_2}{M_1 + M_2} A_0 \\ A'_0 &= \frac{M_1 - M_2}{2M_2} \left(A_0 - A_+ - \frac{q^2}{M_1^2 - M_2^2} A_- \right) \end{aligned} \quad (5.23)$$

and

$$F'_0 = F_+ + \frac{q^2}{M_1^2 - M_2^2} F_-, \quad F'_+ = F_+ \quad (5.24)$$

Once the form factors are known, it is straight forward to calculate the semileptonic decay rates. The differential decay widths are written in terms of helicity amplitudes

Table 5.6: Form factors and associated double pole parameters

F	$F(0)$	a	b	F	$F(0)$	a	b
$A_+^{D \rightarrow K^*}$	0.68	0.86	0.09	$A_-^{D \rightarrow K^{*0}}$	-0.90	0.96	0.14
$A_0^{D \rightarrow K^*}$	2.08	0.40	-0.10	$V^{D \rightarrow K^{*0}}$	0.90	0.97	0.13
$A_+^{D \rightarrow \rho}$	0.57	0.96	0.15	$A_-^{D \rightarrow \rho}$	-0.74	1.11	0.22
$A_0^{D \rightarrow \rho}$	1.47	0.47	-0.10	$V^{D \rightarrow \rho}$	0.76	1.13	0.23
$A_+^{D \rightarrow \omega}$	0.55	1.01	0.17	$A_-^{D \rightarrow \omega}$	-0.69	1.17	0.26
$A_0^{D \rightarrow \omega}$	1.41	0.53	-0.10	$V^{D \rightarrow \omega}$	0.72	1.19	0.27
$A_+^{D_s \rightarrow \phi}$	0.67	1.06	0.17	$A_-^{D_s \rightarrow \phi}$	-0.95	1.20	0.26
$A_0^{D_s \rightarrow \phi}$	2.13	0.59	-0.12	$V^{D_s \rightarrow \phi}$	0.91	1.20	0.25
$A_+^{D_s \rightarrow K^*}$	0.57	1.13	0.21	$A_-^{D_s \rightarrow K^*}$	-0.82	1.32	0.34
$A_0^{D_s \rightarrow K^*}$	1.53	0.61	-0.11	$V^{D_s \rightarrow K^*}$	0.80	1.32	0.33
$F_+^{D \rightarrow K}$	0.77	0.73	0.05	$F_-^{D \rightarrow K}$	-0.39	0.78	0.07
$F_+^{D \rightarrow \pi}$	0.63	0.86	0.09	$F_-^{D \rightarrow \pi}$	-0.41	0.93	0.13
$F_+^{D \rightarrow \eta}$	0.36	0.93	0.12	$F_-^{D \rightarrow \eta}$	-0.20	1.02	0.18
$F_+^{D \rightarrow \eta'}$	0.36	1.23	0.23	$F_-^{D \rightarrow \eta'}$	-0.03	2.29	1.71
$F_+^{D \rightarrow D^0}$	0.91	5.88	4.40	$F_-^{D \rightarrow D^0}$	-0.026	6.32	8.37
$F_+^{D_s \rightarrow \eta}$	0.49	0.69	0.002	$F_-^{D_s \rightarrow \eta}$	-0.26	0.74	0.008
$F_+^{D_s \rightarrow \eta'}$	0.59	0.88	0.018	$F_s^{D_s \rightarrow \eta'}$	-0.23	0.92	0.009
$F_+^{D_s \rightarrow K}$	0.60	1.05	0.18	$F_-^{D_s \rightarrow K}$	-0.38	1.14	0.24
$F_+^{D_s \rightarrow D^0}$	0.92	5.08	2.25	$F_-^{D_s \rightarrow D^0}$	-0.34	6.79	8.91

as

$$\begin{aligned}
 \frac{d\Gamma(D_{(s)} \rightarrow (P, V)\ell^+\nu_\ell)}{dq^2} &= \frac{G_F^2 |V_{cq}|^2 |\mathbf{p}_2| q^2 \left(1 - \frac{m_\ell^2}{q^2}\right)^2}{96\pi^3 M_1^2} \\
 &\times \left[\left(1 + \frac{m_\ell^2}{2q^2}\right) \sum |H_n|^2 + \frac{3m_\ell^2}{2q^2} |H_t|^2 \right], \quad (5.25)
 \end{aligned}$$

with $|\mathbf{p}_2| = \lambda^{1/2}(M_1^2, M_2^2, q^2)/2M_1$ is the momentum of the daughter meson in the rest frame of the $D_{(s)}$ meson and the index n runs through $(+, -, 0)$. The helicity amplitudes are related to the form factors in the following manner:

For $D_{(s)} \rightarrow P$ channel:

$$\begin{aligned}
 H_t &= \frac{1}{\sqrt{q^2}} (PqF_+ + q^2F_-), \\
 H_\pm &= 0 \quad \text{and} \quad H_0 = \frac{2m_1 |\mathbf{p}_2|}{\sqrt{q^2}} F_+ \quad (5.26)
 \end{aligned}$$

For $D_{(s)} \rightarrow V$ channel:

$$\begin{aligned}
H_t &= \frac{1}{m_1 + m_2} \frac{m_1 |\mathbf{p}_2|}{m_2 \sqrt{q^2}} ((m_1^2 - m_2^2)(A_+ - A_-) + q^2 A_-) \\
H_{\pm} &= \frac{1}{m_1 + m_2} (-(m_1^2 - m_2^2)A_0 \pm 2m_1 |\mathbf{p}_2| V) \\
H_0 &= \frac{1}{m_1 + m_2} \frac{1}{2m_2 \sqrt{q^2}} (-(m_1^2 - m_2^2)(m_1^2 - m_2^2 - q^2)A_0 + 4m_1^2 |\mathbf{p}_2|^2 A_+) \quad (5.27)
\end{aligned}$$

For studying the lepton-mass effect, we define the physical observables such as forward-backward asymmetry $\mathcal{A}_{FB}^\ell(q^2)$, the longitudinal $P_L^\ell(q^2)$ and transverse $P_T^\ell(q^2)$ polarization of the charged lepton in the final state. They are also related to the helicity amplitude via the relations

$$\mathcal{A}_{FB}^\ell(q^2) = -\frac{3}{4} \frac{|H_+|^2 - |H_-|^2 + 4\delta_\ell H_0 H_t}{(1 + \delta_\ell) \sum |H_n|^2 + 3\delta_\ell |H_t|^2}, \quad (5.28)$$

$$P_L^\ell(q^2) = -\frac{(1 - \delta_\ell) \sum |H_n|^2 - 3\delta_\ell |H_t|^2}{(1 + \delta_\ell) \sum |H_n|^2 + 3\delta_\ell |H_t|^2}, \quad (5.29)$$

$$P_T^\ell(q^2) = -\frac{3\pi}{4\sqrt{2}} \frac{\sqrt{\delta_\ell} (|H_+|^2 - |H_-|^2 - 2H_0 H_t)}{(1 + \delta_\ell) \sum |H_n|^2 + 3\delta_\ell |H_t|^2}, \quad (5.30)$$

where $\delta_\ell = m_\ell^2/2q^2$ is the helicity-flip factor. The detailed analytical calculations of the helicity amplitudes and differential distributions are given in our recent papers [293, 294, 306, 307]. The averages of these observables in the q^2 range is better suited for experimental measurements with low statistics. In order to compute the averages of these observables Eqns. 5.28 – 5.30, one has to multiply and divide the numerator and denominator with the phase factor $|\mathbf{p}_2|(q^2 - m_\ell^2)^2/q^2$ and integrate separately. These observables are sensitive to contributions of physics beyond the SM and can be used to test LFU violations [308–313].

5.4 Results and Discussion

Having determined all the model parameters we are now in a position to represent our results. First we compute the leptonic branching fractions using the Eq. (5.18) and tabulated in Tab. 5.4. We compare our results with the latest PDG data [1] and it is observed that our results satisfies the experimental constraint for electron channel and for muon and tau channel also our results are in very good agreement with the PDG data.

Then we compute the form factors for the semileptonic decays of $D_{(s)}$ mesons in the entire physical range of momentum transfer. We also compare our findings with the

other theoretical approaches. For comparing our form factors with other studies, we need to transform to BSW form factors Eq. (5.24 and 5.24). We note that based on the method we used in the model-parameter fitting, as well as comparisons of our predictions with experimental data in previous studies, the estimation of the errors for the form factors in our model are of order 20% for small q^2 and 30% for large q^2 .

Table 5.7: Comparison of $F_+(0)$ for $D_{(s)} \rightarrow P$ transitions at maximum recoil.

	$D \rightarrow \pi$	$D \rightarrow K$	$D \rightarrow \eta$	$D \rightarrow \eta'$	$D_s \rightarrow \eta$	$D_s \rightarrow \eta'$	$D_s \rightarrow K^0$
Present	0.63	0.77	0.36	0.36	0.49	0.59	0.60
CQM [280]	0.69	0.78	–	–	0.50	0.60	0.72
LFQM [286]	0.66	0.79	0.39	0.32	0.48	0.59	0.66
LQCD [22]	–	–	–	–	0.564(11)	0.437(18)	–
LQCD [22]	–	–	–	–	0.542(13)	0.404(25)	–
LQCD [17]	0.612(35)	0.765(31)	–	–	–	–	–
LCSR [274]	–	–	0.552 ± 0.051	0.458 ± 0.105	0.432 ± 0.033	0.520 ± 0.080	–
LCSR [276]	–	–	$0.429^{+0.165}_{-0.141}$	$0.292^{+0.113}_{-0.104}$	$0.495^{+0.030}_{-0.029}$	$0.558^{+0.047}_{-0.045}$	–

Table 5.8: Ratios of the $D_{(s)} \rightarrow V$ transition form factors at maximum recoil.

Channel	Ratio	Present	PDG [1]	LQCD [21]	CQM [280]	LFQM [286]	HM χ T [284]
$D \rightarrow \rho$	r_2	0.93	0.83 ± 0.12	–	0.83	0.78	0.51
	r_V	1.26	1.48 ± 0.16	–	1.53	1.47	1.72
$D^+ \rightarrow \omega$	r_2	0.95	1.06 ± 0.16	–	–	0.84	0.51
	r_V	1.24	1.24 ± 0.11	–	–	1.47	1.72
$D \rightarrow K^*$	r_2	0.92	0.80 ± 0.021	–	0.74	0.92	0.5
	r_V	1.22	1.49 ± 0.05	–	1.56	1.26	1.60
$D_s^+ \rightarrow \phi$	r_2	0.99	0.84 ± 0.11	0.74(12)	0.73	0.86	0.52
	r_V	1.34	1.80 ± 0.08	1.72(21)	1.72	1.42	1.80
$D_s^+ \rightarrow K^{*0}$	r_2	0.99	$0.77 \pm 0.28 \pm 0.07$ [314]	–	0.74	0.82	0.55
	r_V	1.40	$1.67 \pm 0.34 \pm 0.16$ [314]	–	1.82	1.55	1.93

In Tab. 5.7, we compare our results of the form factor F_+ at the maximum recoil for the channel $D_{(s)} \rightarrow P$ transition with the other theoretical approaches. It is observed that our results are in very good agreement with the Quark model predictions such as CQM [280] and LFQM [286]. For $D \rightarrow \pi(K)$ channels, our results are in excellent agreement with the LQCD calculations [17,18]. For $D_{(s)} \rightarrow \eta^{(\prime)}$ channels, our results are LCSR [274,276] and LQCD [22] but it is to be noted that the authors of Ref. [22] have considered the LQCD calculations as a pilot study.

For vector form factors, we compare the ratios at the maximum recoil as

$$r_2 = \frac{A_2(0)}{A_1(0)} \quad \text{and} \quad r_V = \frac{V(0)}{A_1(0)} \quad (5.31)$$

In Tab. 5.8, we compare our ratios with the PDG averages data [1] and other theoretical approaches. It is observed that our results for the ratios of the form factors agree well with the PDG data within the uncertainty except for the channel $D_s \rightarrow \phi$. It is also important to note that our result $r_V(D_s \rightarrow \phi) = 1.34$ is very close to the value 1.42 from LFQM [286].

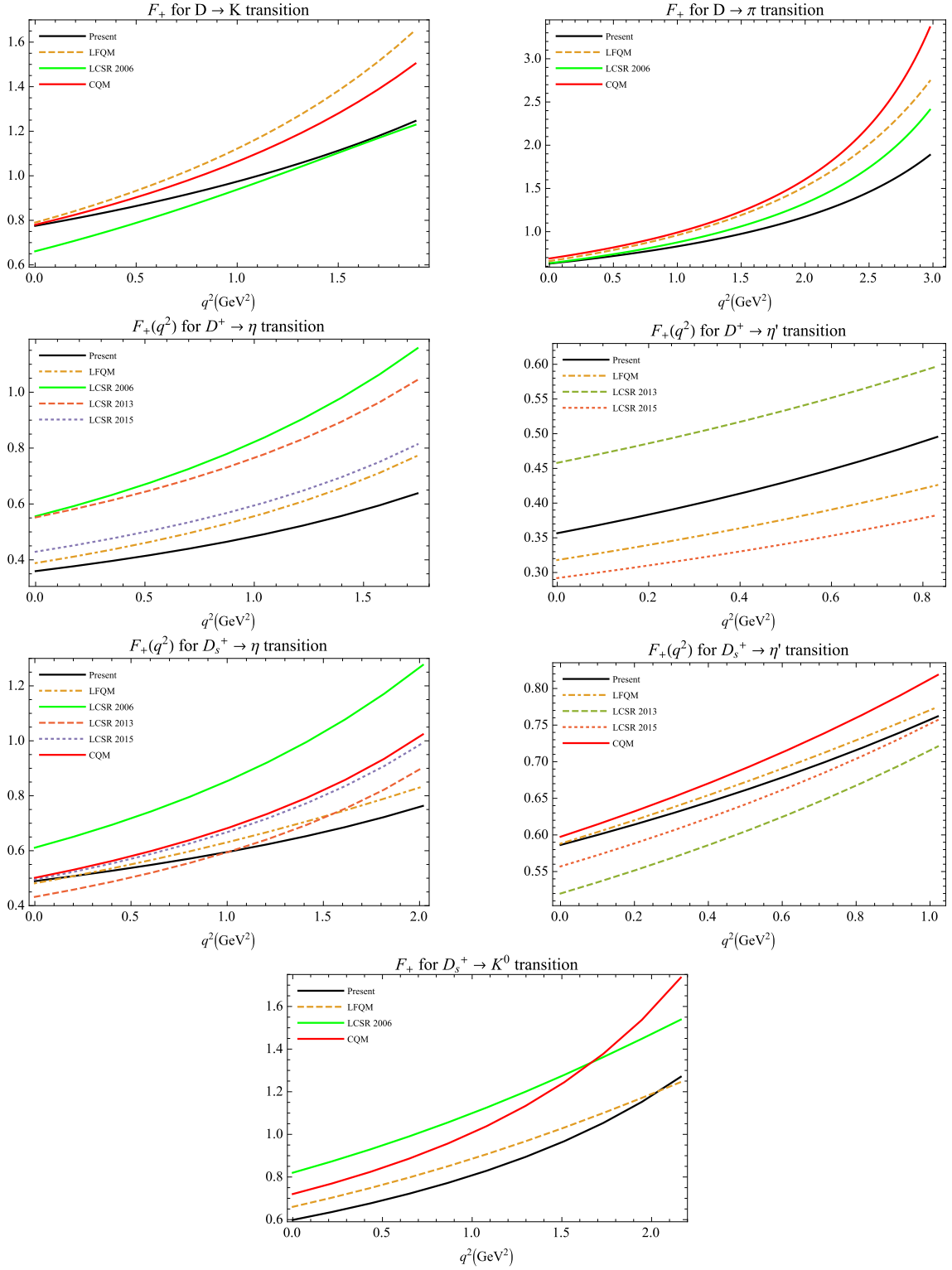


Figure 5.4: The form factors for semileptonic $D \rightarrow K, \pi$, $D_{(s)}^+ \rightarrow \eta^{(\prime)}$ and $D_s^+ \rightarrow K^0$ transitions with comparison to LCSR, LFQM and CQM.

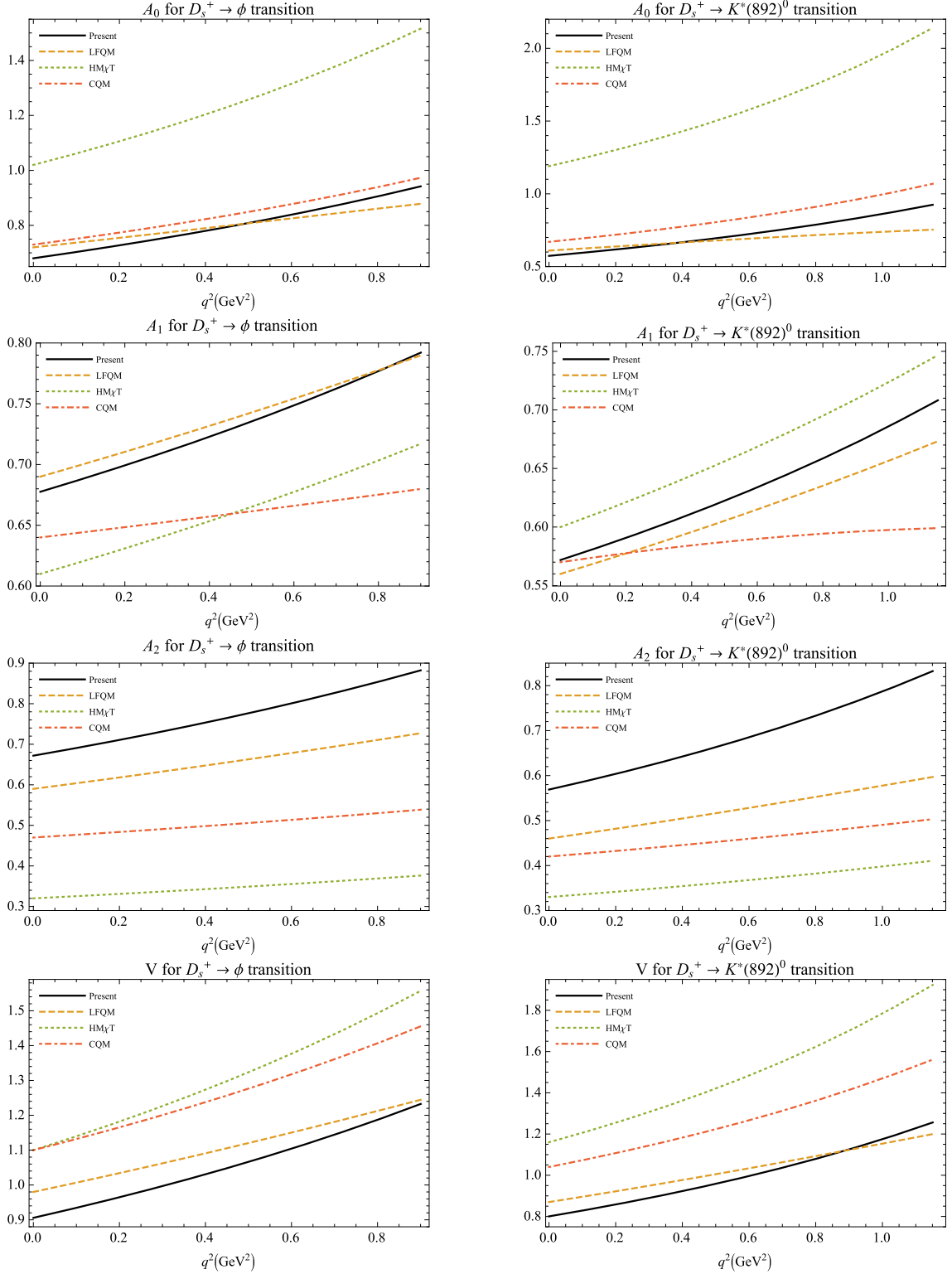


Figure 5.5: The form factors for semileptonic $D_s^+ \rightarrow \phi$ (left) and $D_s^+ \rightarrow K^*(892)^-$ (right) transitions with comparison to LFQM, $HM_\chi T$ and CQM.

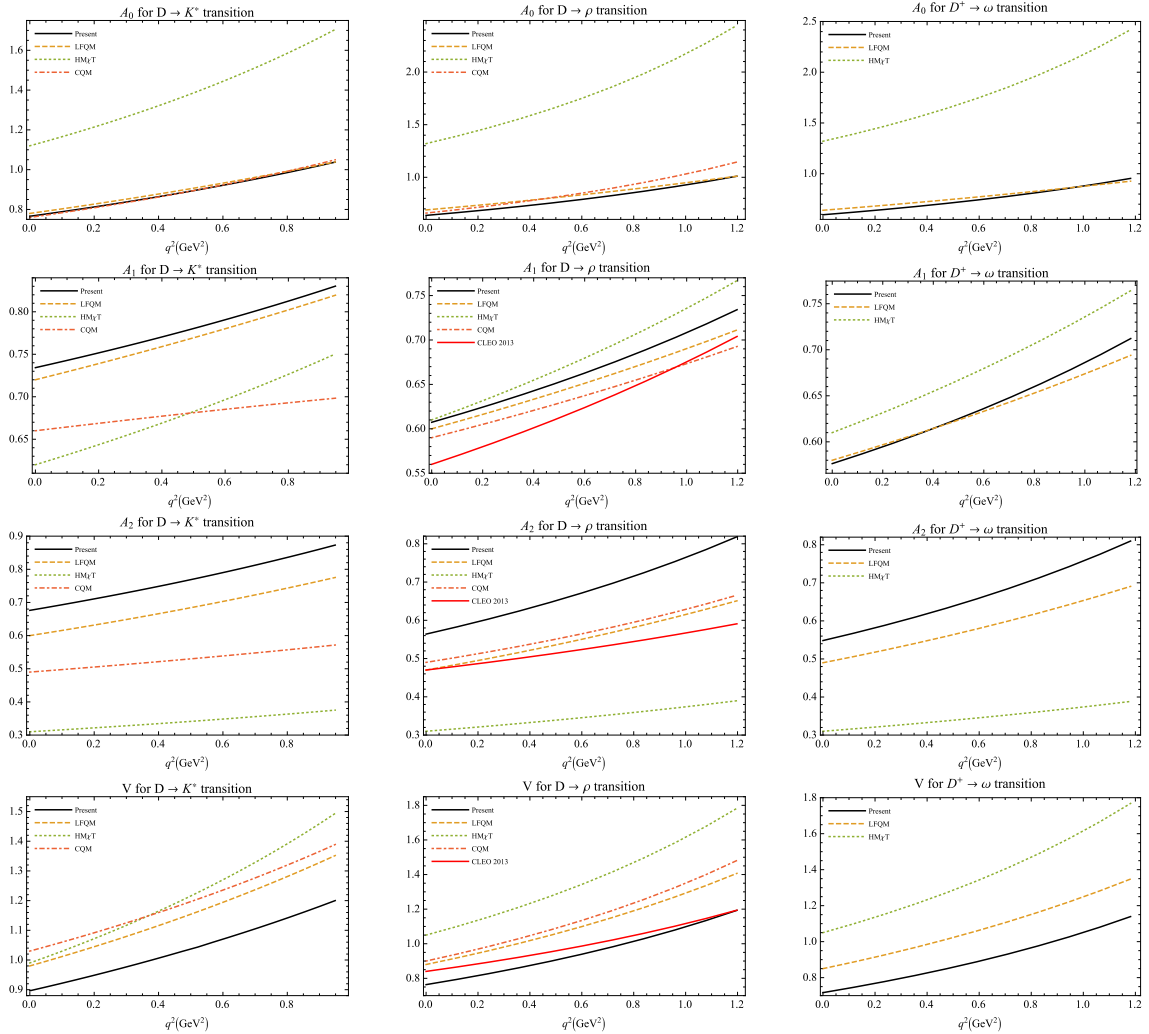


Figure 5.6: The form factors for semileptonic $D^+ \rightarrow K^*$ (left), $D \rightarrow \rho$ (middle) and $D \rightarrow \omega$ (right) transitions with comparison to LFQM, $\text{HM}\chi\text{T}$, CQM and CLEO data.

In Figs. 5.4 – 5.6 we plot the form factors in the entire q^2 range of momentum transfer i.e. $0 \leq q^2 \leq q_{max}^2 = (m_{D(s)} - m_{P/V})^2$. It is interesting to note that our results are in excellent agreement with the LFQM [286] for all the channels. It is also observed that the $\text{HM}\chi\text{T}$ [284] predictions for the $A_0(q^2)$ is much higher than the other theoretical calculations.

It is important to note that the form factor computation to the η and η' channel is different since they are the mixture of s -quark and light quarks component. The quark content in the approximation of $m_u = m_d \equiv m_q$ can be written as [315]

$$\begin{pmatrix} \eta \\ \eta' \end{pmatrix} = - \begin{pmatrix} \sin \delta & \cos \delta \\ -\cos \delta & \sin \delta \end{pmatrix} \begin{pmatrix} q\bar{q} \\ s\bar{s} \end{pmatrix}, \quad q\bar{q} \equiv \frac{u\bar{u} + d\bar{d}}{\sqrt{2}}. \quad (5.32)$$

The angle δ is defined by $\delta = \theta_P - \theta_I$, where $\theta_I = \arctan(1/\sqrt{2})$ is the ideal mixing

angle. We adopt the value $\theta_P = -15.4^\circ$ from Ref. [315]. Also, in computing the form factors for the channel $D \rightarrow \eta^{(\prime)}$, we take the contribution from the $q\bar{q}$ component while for the $D_s \rightarrow \eta^{(\prime)}$ channel, we take the contribution from the $s\bar{s}$ component only [285].

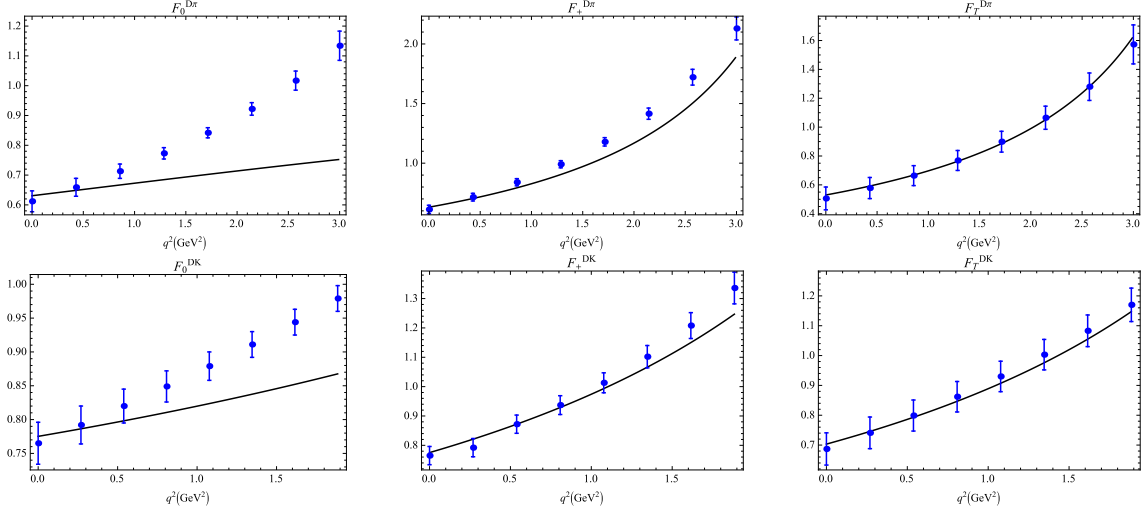


Figure 5.7: $D \rightarrow \pi(K)$ form factors obtained in our model (solid lines) and in LQCD calculations (dots with error bar) by ETM collaboration.

Table 5.9: $D \rightarrow \pi(K)\ell\nu$ form factors and their ratios at $q^2 = 0$.

	$f_+^{D\pi}$	f_+^{DK}	$f_T^{D\pi}$	f_T^{DK}	$f_T^{D\pi}/f_+^{D\pi}$	f_T^{DK}/f_+^{DK}
Present	0.63	0.78	0.53	0.70	0.84	0.90
ETM [17, 18]	0.612(35)	0.765(31)	0.506(79)	0.687(54)	0.827(114)	0.898(50)

Recently, ETM collaboration has provided the LQCD calculations [17, 18] for the full set of form factors for the channel $D \rightarrow \pi(K)\ell\nu_\ell$ and $D \rightarrow \pi(K)\ell\ell$ including tensor and scalar form factors. The tensor form factor is defined as

$$\langle P(p_2) | \bar{q} \sigma^{\mu\nu} (1 - \gamma^5) c | D(p_1) \rangle = \frac{iF^T(q^2)}{M_1 + M_2} (P^\mu q^\nu - P^\nu q^\mu + i\varepsilon^{\mu\nu Pq}). \quad (5.33)$$

and the scalar form factor $F_0(q^2)$ can be computed using $F_+(q^2)$ and $F_-(q^2)$ defined in Eq. (5.20)

$$F_0(q^2) = F_+(q^2) + \frac{q^2}{M_1^2 - M_2^2} F_-(q^2). \quad (5.34)$$

In Fig. 5.7, we compare our form factors for the channel $D \rightarrow \pi(K)$ with the LQCD data by ETM Collaboration. It is observed that our plot for $F_0(q^2)$ agrees well with ETM in low q^2 region. However, our plot for $F_+(q^2)$ is very close to ETM and the tensor form factors are in excellent agreement with ETM. In Tab. 5.9, we

also present our results of the form factors at the maximum recoil along with the comparison with ETM. It is worth noting that our results agree well with ETM calculations within the uncertainties.

Next we compute the semileptonic branching fractions. In Tab. 5.10 – 5.12, we summarize our outcomes with the other theoretical approaches and the recent data given by CLEO and BESIII collaborations.

Table 5.10: Semileptonic decays of D^0 mesons (in %)

Channel	Present	Other	Reference	Data	Reference
$D^0 \rightarrow K^- e^+ \nu_e$	3.63	3.4	HM χ T [283]	$3.505 \pm 0.014 \pm 0.033$ $3.50 \pm 0.03 \pm 0.04$ $3.45 \pm 0.07 \pm 0.20$	BESIII [316] CLEO [270] Belle [268]
$D^0 \rightarrow K^- \mu^+ \nu_\mu$	3.53			$3.413 \pm 0.019 \pm 0.035$	BESIII [317]
$D^0 \rightarrow \pi^- e^+ \nu_e$	0.22	0.27	HM χ T [283]	$0.295 \pm 0.004 \pm 0.003$ $0.2770 \pm 0.0068 \pm 0.0092$ $0.288 \pm 0.008 \pm 0.003$ $0.255 \pm 0.019 \pm 0.016$	BESIII [316] <i>BABAR</i> [266] CLEO [270] Belle [268]
$D^0 \rightarrow \pi^- \mu^+ \nu_\mu$	0.22			$0.272 \pm 0.008 \pm 0.006$	BESIII [318]
$D^0 \rightarrow K^*(892)^- e^+ \nu_e$	2.96	2.15 2.2	χ UA [288] HM χ T [284]	$2.033 \pm 0.046 \pm 0.047$ $2.16 \pm 0.15 \pm 0.08$	BESIII [319] CLEO [320]
$D^0 \rightarrow K^*(892)^- \mu^+ \nu_\mu$	2.80	1.98	χ UA [288]		
$D^0 \rightarrow \rho^- e^+ \nu_e$	0.16	0.197 $0.1749^{+0.0421}_{-0.0297}$ 0.20	χ UA [288] LCSR HM χ T [284]	$0.1445 \pm 0.0058 \pm 0.0039$ $0.177 \pm 0.012 \pm 0.010$	BESIII [321] CLEO [322] [278]
$D^0 \rightarrow \rho^- \mu^+ \nu_\mu$	0.15	0.1 0.184	ISGW2 [323] χ UA [288]	–	–

In Tab. 5.10, we summarize our results for $D^0 \rightarrow (P, V)\ell^+\nu_\ell$ channel. The following are our comments:

- For $D^0 \rightarrow K^- \ell^+ \nu_\ell$ channel, our results are in very good agreement with the recent BESIII data also with the CLEO and Belle data.
- For $D^0 \rightarrow K^*(892)^-$ channel, our results are higher than the CLEO data for the electrono channel and for still experimental results are still not available.
- For $D^0 \rightarrow \pi^-$ channel, our results are higher than the recent BESIII data but it is nearer to the data from Belle results.
- For $D^0 \rightarrow \rho^- e^+ \nu_e$ channel, our results are matching very well with the central values of the CLEO data [322].

In Tab. 5.11 we summarize our results on $D^+ \rightarrow (P, V)\ell^+\nu_\ell$ channels. Our results are in good agreement with the experimental data. The following are our comments:

- For $D^+ \rightarrow \bar{K}^0 \ell^+ \nu_\ell$ channel, our results are nearly 8 % higher than the BESIII data.

Table 5.11: Semileptonic decays of D^+ mesons

Channel	Unit	Present	Other	Reference	Data	Reference
$D^+ \rightarrow \bar{K}^0 e^+ \nu_e$	10^{-2}	9.28	8.4	HM χ T [283]	$8.60 \pm 0.06 \pm 0.15$	BESIII [324]
			10.32 ± 0.93	LFQM [287]	$8.83 \pm 0.10 \pm 0.20$	CLEO [270]
$D^+ \rightarrow \bar{K}^0 \mu^+ \nu_\mu$	10^{-2}	9.02	10.07 ± 0.91	LFQM [287]	$8.72 \pm 0.07 \pm 0.18$	BESIII [325]
$D^+ \rightarrow \pi^0 e^+ \nu_e$	10^{-2}	0.29	0.33	HM χ T [283]	$0.350 \pm 0.011 \pm 0.010$	BESIII [318]
			0.41 ± 0.03	LFQM [287]		
$D^+ \rightarrow \pi^0 \mu^+ \nu_\mu$	10^{-2}	0.28	0.41 ± 0.03	LFQM [287]		
$D^+ \rightarrow \bar{K}^{*0}(892) e^+ \nu_e$	10^{-2}	7.61	5.56	χ UA [288]		
			5.6	HM χ T [284]		
$D^+ \rightarrow \bar{K}^{*0}(892) \mu^+ \nu_\mu$	10^{-2}	7.21	5.12	χ UA [288]		
$D^+ \rightarrow \rho^0 e^+ \nu_e$	10^{-3}	2.09	2.54	χ UA [288]	$1.860 \pm 0.070 \pm 0.061$	BESIII [321]
			$2.217^{+0.534}_{-0.376} \pm 0.015$	LCSR [278]	$2.17 \pm 0.12^{+0.12}_{-0.22}$	CLEO [322]
			2.5	HM χ T [284]		
$D^+ \rightarrow \rho^0 \mu^+ \nu_\mu$	10^{-3}	2.01	2.37	χ UA [288]	2.4 ± 0.4	PDG [1]
$D^+ \rightarrow \omega e^+ \nu_e$	10^{-3}	1.85	2.46	χ UA [288]	$1.63 \pm 0.11 \pm 0.08$	BESIII [316]
			2.5	HM χ T [284]	$1.82 \pm 0.18 \pm 0.07$	CLEO [322]
			2.1 ± 0.2	LFQM [287]		
$D^+ \rightarrow \omega \mu^+ \nu_\mu$	10^{-3}	1.78	2.29	χ UA [288]	–	–
			2.0 ± 0.2	LFQM [287]		
$D^+ \rightarrow \eta e^+ \nu_e$	10^{-4}	9.38	12 ± 1	LFQM [287]	$10.74 \pm 0.81 \pm 0.51$	BESIII [326]
			24.5 ± 5.26	LCSR [274]	$11.4 \pm 0.9 \pm 0.4$	CLEO [327]
			14.24 ± 10.98	LCSR [276]		
$D^+ \rightarrow \eta \mu^+ \nu_\mu$	10^{-4}	9.12	12 ± 1	LFQM [287]	–	–
$D^+ \rightarrow \eta' e^+ \nu_e$	10^{-4}	2.00	1.8 ± 0.2	LFQM [287]	$1.91 \pm 0.51 \pm 0.13$	BESIII [326]
			3.86 ± 1.77	LCSR [274]	$2.16 \pm 0.53 \pm 0.07$	CLEO [327]
			1.52 ± 1.17	LCSR [276]		
$D^+ \rightarrow \eta' \mu^+ \nu_\mu$	10^{-4}	1.90	1.7 ± 0.2	LFQM [287]	–	–

- For $D^+ \rightarrow \bar{K}^{*0}(892) \ell^+ \nu_\ell$ channel, still the experimental results are not available. Also our results are nearer to the other theoretical approaches.
- $D^+ \rightarrow \pi^0 \ell^+ \nu_\ell$ channel, our results are very well within the range predicted by the BESIII data.
- For $D^+ \rightarrow \omega e^+ \nu_e$ channel, our result is a bit higher than the BESIII data [316], but it is well within the range predicted by CLEO data [322].
- For $D^+ \rightarrow \eta^{(\prime)}$ channel, the branching fractions are very small and also wide range of uncertainties have been reported in the experiments. Our results remain within the range predicted by recent BESIII data [326] and also with the results on CLEO data [328]. We also compare our results with the results from LCSR data [274] and [276].
- We have compared our results with the other theoretical approaches such as LCSR [274, 276, 278], χ UA [288], LFQM [287], HM χ T [283] and ISGW2 [323]. Our results for $D \rightarrow \rho e^+ \nu_e$ give very good agreement with the LCSR [278] and χ UA [288] results. For muon channel also, our results are very nearer to those obtained in χ UA [288]. For $D^+ \rightarrow \omega \ell^+ \nu_\ell$ channel, our results are matching with the LFQM [287]. For $D^+ \rightarrow \eta^{(\prime)} \ell^+ \nu_\ell$ channel, our results are deviating from the results obtained in LCSR [274, 276], but are very close to the LFQM data [287].

In Tab 5.12, we summarize the results on $D_s \rightarrow (P, V) \ell \nu_\ell$ channels. The short

Table 5.12: Semileptonic branching fractions of D_s mesons (in %).

Channel	Present	Other	Reference	Experimental Data	Reference
$D_s^+ \rightarrow \phi e^+ \nu_e$	3.01	2.12	χ UA [288]	$2.26 \pm 0.45 \pm 0.09$	BESIII [329]
		3.1 ± 0.3	LFQM [287]	$2.61 \pm 0.03 \pm 0.08 \pm 0.15$	<i>BABAR</i> [267]
		2.4	HM χ T [284]	$2.14 \pm 0.17 \pm 0.08$	CLEO [328]
$D_s^+ \rightarrow \phi \mu^+ \nu_\mu$	2.85	1.94	χ UA [288]	$1.94 \pm 0.53 \pm 0.09$	BESIII [329]
		2.9 ± 0.3	LFQM [287]		
$D_s^+ \rightarrow K^0 e^+ \nu_e$	0.20	0.27 ± 0.02	LFQM [287]	$0.39 \pm 0.08 \pm 0.03$	CLEO [328]
$D_s^+ \rightarrow K^0 \mu^+ \nu_\mu$	0.19	0.26 ± 0.02	LFQM [287]	–	
$D_s^+ \rightarrow K^*(892)^0 e^+ \nu_e$	0.18	0.202	χ UA [288]	$0.18 \pm 0.04 \pm 0.01$	CLEO [328]
		0.19 ± 0.02	LFQM [287]		
		0.22	HM χ T [284]		
$D_s^+ \rightarrow K^*(892)^0 \mu^+ \nu_\mu$	0.17	0.189	χ UA [288]	–	–
		0.19 ± 0.02	LFQM [287]		
$D_s^+ \rightarrow \eta e^+ \nu_e$	2.24	2.26 ± 0.21	LFQM [287]	$2.30 \pm 0.31 \pm 0.08$	BESIII [330]
		2.0 ± 0.32	LCSR [274]	$2.28 \pm 0.14 \pm 0.19$	CLEO [328]
		2.40 ± 0.28	LCSR [276]		
$D_s^+ \rightarrow \eta \mu^+ \nu_\mu$	2.18	2.22 ± 0.20	LFQM [287]	$2.42 \pm 0.46 \pm 0.11$	BESIII [329]
$D_s^+ \rightarrow \eta' e^+ \nu_e$	0.83	0.89 ± 0.09	LFQM [287]	$0.93 \pm 0.30 \pm 0.05$	BESIII [330]
		0.75 ± 0.23	LCSR [274]	$0.68 \pm 0.15 \pm 0.06$	CLEO [328]
		0.79 ± 0.14	LCSR [276]		
$D_s^+ \rightarrow \eta' \mu^+ \nu_\mu$	0.79	0.85 ± 0.08	LFQM [287]	$1.06 \pm 0.54 \pm 0.07$	BESIII [329]

comments are:

- For $D_s^+ \rightarrow \phi \ell^+ \nu_\ell$ channel, our result is quite high compared to recent BESIII [329] and the results based on CLEO [328] data but it is observed to be within the range predicted by *BABAR* data [267].
- For $D_s^+ \rightarrow K^0 \ell^+ \nu_\ell$ channel, our result for branching fraction is almost double with compared to CLEO data [328]. For electron and muon channels, experimental results are yet to be reported. Our result for the channel $D_s^+ \rightarrow K^*(892)^0 e^+ \nu_e$ is matching perfectly with the central value of the CLEO data [328]. The discrepancy of our results with the experimental results seems obvious as there are large deviations of the form factors, particularly A_0 and A_2 in the Figs. 5.5 and f_+ in the last plot in Fig. 5.4.
- For $D_s^+ \rightarrow \eta^{(\prime)} \ell^+ \nu_\ell$, there is wide range of uncertainties reported in the experimental data and LCSR results. Our results are in excellent agreement with the BESIII [330] and CLEO [328] results for the electron channel. For muonic channel, our results give excellent agreement with the BESIII data [326] which is a first time ever experimental observation.
- Here also we compare our findings with the theoretical models such as χ UA [288], LCSR [274, 276], HM χ T [284] and LFQM [287]. For $D_s^+ \rightarrow \phi \ell^+ \nu_\ell$ channel, though our result is higher than BESIII and *BABAR* data, it is in good agreement with the LFQM [287] data. But for the $D_s^+ \rightarrow K^0 \ell^+ \nu_\ell$ channel, our result is lower than the LFQM predictions. For the rest of the D_s^+ semileptonic decays, our results are in good accordance with the LFQM [287] and LCSR [274, 276] predictions.

Overall, our results are in very good agreement with the experimental results along with theoretical models such as LFQM and LCSR predictions. In Tab. 5.13, we

Table 5.13: Ratios of the semileptonic decays

Ratio	SM	Value	Data	Reference
$\Gamma(D^0 \rightarrow K^- e^+ \nu_e)/\Gamma(D^+ \rightarrow \bar{K}^0 e^+ \nu_e)$	1.0	0.99	$1.08 \pm 0.22 \pm 0.07$ $1.06 \pm 0.02 \pm 0.03$	BESIII [331] CLEO [332]
$\Gamma(D^0 \rightarrow K^- \mu^+ \nu_\mu)/\Gamma(D^+ \rightarrow \bar{K}^0 \mu^+ \nu_\mu)$	1.0	0.99		
$\Gamma(D^+ \rightarrow \bar{K}^0 \mu^+ \nu_\mu)/\Gamma(D^+ \rightarrow \bar{K}^0 e^+ \nu_e)$	1.0	0.97		
$\Gamma(D^0 \rightarrow K^- \mu^+ \nu_\mu)/\Gamma(D^0 \rightarrow K^- e^+ \nu_e)$	1.0	0.97	$0.974 \pm 0.007 \pm 0.012$	BESIII [317]
$\mathcal{B}(D^0 \rightarrow \pi^- \mu^+ \nu_\mu)/\mathcal{B}(D^0 \rightarrow \pi^- e^+ \nu_e)$	1.0	0.98	$0.922 \pm 0.030 \pm 0.022$	BESIII [318]
$\mathcal{B}(D^+ \rightarrow \pi^0 \mu^+ \nu_\mu)/\mathcal{B}(D^+ \rightarrow \pi^0 e^+ \nu_e)$	1.0	0.98	$0.964 \pm 0.037 \pm 0.026$	BESIII [318]
$\Gamma(D^0 \rightarrow \pi^- e^+ \nu_e)/\Gamma(D^+ \rightarrow \pi^0 e^+ \nu_e)$	2.0	1.97	$2.03 \pm 0.14 \pm 0.08$	CLEO [332]
$\Gamma(D^0 \rightarrow \rho^- e^+ \nu_e)/2\Gamma(D^+ \rightarrow \rho^0 e^+ \nu_e)$	1.0	0.98	$1.03 \pm 0.09^{+0.08}_{-0.02}$	CLEO [322]
$\mathcal{B}(D^+ \rightarrow \eta' e^+ \nu_e)/\mathcal{B}(D^+ \rightarrow \eta e^+ \nu_e)$	-	0.21	0.19 ± 0.05 0.18 ± 0.05	CLEO [327] BESIII [326]
$\mathcal{B}(D_s^+ \rightarrow \phi \mu^+ \nu_\mu)/\mathcal{B}(D_s^+ \rightarrow \phi e^+ \nu_e)$	1.0	0.95	0.86 ± 0.29	BESIII [329]
$\mathcal{B}(D_s^+ \rightarrow \eta' e^+ \nu_e)/\mathcal{B}(D_s^+ \rightarrow \eta e^+ \nu_e)$	-	0.37	0.36 ± 0.14 0.40 ± 0.14	CLEO [333] BESIII [330]
$\mathcal{B}(D_s^+ \rightarrow \eta' \mu^+ \nu_\mu)/\mathcal{B}(D_s^+ \rightarrow \eta \mu^+ \nu_\mu)$	-	0.36	0.44 ± 0.23	BESIII [329]

present the ratios of different semileptonic decay widths. It is observed that our results are very well within the isospin conservation rules [334]. It is worth mentioning here that very recently, the BESIII collaboration has reported their measurement of $\mathcal{B}(D^0 \rightarrow K^- \mu^+ \nu_\mu)$ [317] with significantly improved precision and they also approved our prediction of the model for the channel $\mathcal{B}(D^0 \rightarrow K^- \mu^+ \nu_\mu)/\mathcal{B}(D^0 \rightarrow K^- e^+ \nu_e)$ provided in our paper Ref. [293].

Table 5.14: Semileptonic branching fractions for $D_{(s)}^+ \rightarrow D^0 \ell^+ \nu_\ell$

Channel	Present	Theory Data	Reference	Experimental Data	Reference
$D^+ \rightarrow D^0 e^+ \nu_e$	2.23×10^{-13}	2.78×10^{-13} 2.71×10^{-13}	[291] [292]	$< 1.0 \times 10^{-4}$	BESIII [290]
$D_s^+ \rightarrow D^0 e^+ \nu_e$	2.52×10^{-8}	$(2.97 \pm 0.03) \times 10^{-8}$ 3.34×10^{-8}	[291] [292]	-	-

In Tab. 5.14, we present our results on the rare semileptonic branching fractions of $D_{(s)}^+ \rightarrow D^0 e^+ \nu_e$. Our results for branching fraction for the channel $D^+ \rightarrow D^0 e^+ \nu_e$ satisfies the experimental constraints predicted by the recent BESIII [290] collaboration. Our results also satisfies the theoretical predictions using SU(3) symmetry [291] and also heavy flavour conserving decays [292].

Finally, in Table 5.15 we list our predictions for the forward-backward asymmetry $\langle \mathcal{A}_{FB}^\ell \rangle$, the longitudinal polarization $\langle P_L^\ell \rangle$, and the transverse polarization $\langle P_T^\ell \rangle$ of the charged lepton in the final state. It is seen that for the $P \rightarrow V$ transitions, the

Table 5.15: Forward-backward asymmetry and longitudinal polarization.

Channel	$\langle \mathcal{A}_{FB}^e \rangle$	$\langle \mathcal{A}_{FB}^\mu \rangle$	$\langle P_L^e \rangle$	$\langle P_L^\mu \rangle$
$D^0 \rightarrow K^- \ell^+ \nu_\ell$	-6.14×10^{-6}	-0.06	-1.00	-0.87
$D^0 \rightarrow K^*(892)^- \ell^+ \nu_\ell$	0.18	0.14	-1.00	-0.92
$D^0 \rightarrow \pi^- \ell^+ \nu_\ell$	-3.84×10^{-6}	-0.04	-1.00	-0.90
$D^0 \rightarrow \rho^- \ell^+ \nu_\ell$	0.21	0.18	-1.00	-0.92
$D^+ \rightarrow K^0 \ell^+ \nu_\ell$	-6.11×10^{-6}	-0.06	-1.00	-0.87
$D^+ \rightarrow \bar{K}^*(892)^- \ell^+ \nu_\ell$	0.18	0.14	-1.00	-0.92
$D^+ \rightarrow \pi^0 \ell^+ \nu_\ell$	-3.80×10^{-6}	-0.04	-1.00	-0.91
$D^+ \rightarrow \rho^0 \ell^+ \nu_\ell$	0.22	0.19	-1.00	-0.93
$D^+ \rightarrow \omega \ell^+ \nu_\ell$	0.21	0.18	-1.00	-0.93
$D^+ \rightarrow \eta \ell^+ \nu_\ell$	-6.18×10^{-6}	-0.06	-1.00	-0.87
$D^+ \rightarrow \eta' \ell^+ \nu_\ell$	-13.23×10^{-6}	-0.10	-1.00	-0.82
$D^+ \rightarrow D^0 \ell^+ \nu_\ell$	-0.094	-	-0.73	-
$D_s^+ \rightarrow \phi \ell^+ \nu_\ell$	0.18	0.14	-1.00	-0.92
$D_s^+ \rightarrow K^{*0} \ell^+ \nu_\ell$	0.22	0.19	-1.00	-0.93
$D_s^+ \rightarrow K^0 \ell^+ \nu_\ell$	-4.75×10^{-6}	-0.05	-1.00	-0.89
$D_s^+ \rightarrow \eta \ell^+ \nu_\ell$	-5.75×10^{-6}	-0.06	-1.00	-0.87
$D_s^+ \rightarrow \eta' \ell^+ \nu_\ell$	11.20×10^{-6}	-0.09	-1.00	-0.83
$D_s^+ \rightarrow D^0 \ell^+ \nu_\ell$	-5.33×10^{-4}	-	-1.00	-

lepton-mass effect in $\langle \mathcal{A}_{FB}^\ell \rangle$ is small, resulting in a difference of only 10% – 15% between the corresponding electron and muon modes. For the $P \rightarrow P'$ transitions, $\langle \mathcal{A}_{FB}^\mu \rangle$ are about 10^4 times larger than $\langle \mathcal{A}_{FB}^e \rangle$. This is readily seen from Eq. (5.28): for $P \rightarrow P'$ transitions the two helicity amplitudes H_\pm vanish and the forward-backward asymmetry is proportional to the lepton mass squared. Regarding the longitudinal polarization, the difference between $\langle P_L^\mu \rangle$ and $\langle P_L^e \rangle$ is 10% – 30%. One sees that the lepton-mass effect in the transverse polarization is much more significant than that in the longitudinal one. This is true for both $P \rightarrow P'$ and $P \rightarrow V$ transitions. Note that the values of $\langle \mathcal{A}_{FB}^e \rangle$ and $\langle P_{L(T)}^e \rangle$ for the rare decays $D_{(s)}^+ \rightarrow D^0 e^+ \nu_e$ are quite different in comparison with other $P \rightarrow P'$ transitions due to their extremely small kinematical regions.

We expect BESIII and other experiments such as LHC-b, Belle, CLEO and PANDA collaborations to throw more light in search of these transitions.